GEOPHYSICS, VOL. 69, NO. 3 (MAY-JUNE 2004); P. 708–718, 17 FIGS.
10.1190/1.1759457

Migration velocity analysis in factorized VTI media

Debashish Sarkar* and Ilya Tsvankin‡

ABSTRACT

One of the main challenges in anisotropic velocity analysis and imaging is simultaneous estimation of velocity gradients and anisotropic parameters from reflection data. Approximating the subsurface by a factorized VTI (transversely isotropic with a vertical symmetry axis) medium provides a convenient way of building vertically and laterally heterogeneous anisotropic models for prestack depth migration.

The algorithm for P-wave migration velocity analysis (MVA) introduced here is designed for models composed of factorized VTI layers or blocks with constant vertical and lateral gradients in the vertical velocity V_{P0}. The anisotropic MVA method is implemented as an iterative two-step procedure that includes prestack depth migration (imaging step) followed by an update of the medium parameters (velocity-analysis step). The residual moveout of the migrated events, which is minimized during the parameter updates, is described by a nonhyperbolic equation whose coefficients are determined by 2D semblance scanning.

For piecewise-factorized VTI media without significant dips in the overburden, the residual moveout of P-wave events in image gathers is governed by four effective quantities in each block: (1) the normal-moveout velocity $V_{\rm nmo}$ at a certain point within the block, (2) the vertical velocity gradient k_z, (3) the combination $\hat{k}_x = k_x\sqrt{1+2\delta}$ of the lateral velocity gradient k_x and the anisotropic parameter δ, and (4) the anellipticity parameter η. We show that all four parameters can be estimated from the residual moveout for at least two reflectors within a block sufficiently separated in depth. Inversion for the parameter η also requires using either long-spread data (with the maximum offset-to-depth ratio no less than two) from horizontal interfaces or reflections from dipping interfaces.

To find the depth scale of the section and build a model for prestack depth migration using the MVA results, the vertical velocity V_{P0} needs to be specified for at least a single point in each block. When no borehole information about V_{P0} is available, a well-focused image can often be obtained by assuming that the vertical-velocity field is continuous across layer boundaries. A synthetic test for a three-layer model with a syncline structure confirms the accuracy of our MVA algorithm in estimating the interval parameters $V_{\rm nmo}$, k_z, $\hat{k}_x$, and η and illustrates the influence of errors in the vertical velocity on the image quality.

INTRODUCTION

Most existing velocity-analysis methods for transversely isotropic media with a vertical symmetry axis (VTI) approximate the subsurface with homogeneous layers or blocks (e.g., Alkhalifah and Tsvankin, 1995; Le Stunff and Jeannot, 1998; Tsvankin, 2001; Grechka et al., 2002). Anisotropic layers, however, are often characterized by nonnegligible lateral and vertical velocity gradients that may distort the shape of underlying reflectors and cause errors in the anisotropic parameters. Alkhalifah (1997) and Han et al. (2000) introduced time-domain velocity-analysis algorithms for vertically heterogeneous VTI models. However, their approach is not designed to reconstruct the spatially varying vertical velocity and, therefore, is not directly applicable to depth imaging. In particular, depth migration has to account properly for lateral variations of the velocity field.

An analytic correction of normal-moveout (NMO) ellipses for lateral velocity variation in anisotropic media was developed by Grechka and Tsvankin (1999). Their method, however, is limited to horizontal layers, small lateral velocity gradients, and the hyperbolic portion of reflection moveout. Also, for purposes of depth imaging, we are interested in estimating lateral velocity variation rather than just removing its influence on anisotropic inversion. The main problem in reconstructing a spatially varying anisotropic velocity field is caused by the trade-offs between the velocity gradients, anisotropic parameters, and the shapes of the reflecting

Manuscript received by the Editor August 4, 2003; revised manuscript received February 3, 2004.
*Formerly Colorado School of Mines, Department of Geophysics, Golden, Colorado 80401-1887; presently GX Technology, 5847 San Felipe, Suite 3800, Houston, Texas 77057. E-mail: dsarkar@gxt.com.
‡Colorado School of Mines, Center for Wave Phenomena, Golden, Colorado 80401-1887. E-mail: ilya@dix.mines.edu.

interfaces. Even in isotropic media, some trade-offs between the velocity field and reflector shapes cannot be resolved without a priori information.

A practical way to incorporate vertical and lateral velocity variations into anisotropic velocity analysis without excessively compromising the uniqueness of the solution is to adopt the so-called factorized anisotropic model in which the ratios of the stiffness coefficients (and, therefore, the anisotropic parameters) are constant. Here, we consider a model composed of factorized VTI blocks, where each block is bounded by plane or irregular interfaces. The problem is treated in two dimensions, which implies that the vertical incidence plane that contains sources and receivers should coincide with the dip plane of the subsurface structure. The vertical P-wave velocity V_{P0} is assumed to vary linearly within each block, so the vertical (k_z) and lateral (k_x) gradients in V_{P0} are constant. The kinematics of P-wave propagation in each block can be described by five parameters: the velocity V_{P0} defined at a certain spatial location, the gradients k_z and k_x, and the Thomsen (1986) anisotropic parameters ϵ and δ. Although it is possible to introduce jumps in velocity across the boundaries of the blocks, piecewise factorized media can be conveniently used to generate smooth velocity fields required by many migration algorithms (in particular, those based on ray tracing).

A generalized version of the factorized model was introduced by Alkhalifah et al. (2001), who considered heterogeneous VTI media where the ratio of the P-wave NMO and vertical velocity is laterally invariant. Under this assumption, the ray tracing and eikonal equations in the midpoint (x) vertical-traveltime (τ) coordinates become independent of the vertical velocity, and time processing is governed by only the NMO velocity and the Alkahlifah and Tsvankin (1995) parameter $\eta \equiv (\epsilon - \delta)/(1 + 2\delta)$. The methodology of Alkhalifah et al. (2001), however, is not directly applicable to prestack depth imaging because in the x-τ domain different vertically heterogeneous models cannot be distinguished from one another.

Since our goal is to estimate the relevant VTI parameters and carry out depth imaging for models with significant lateral and vertical velocity variation, velocity model building is conveniently implemented in the prestack depth-migrated domain (e.g., Stork, 1992; Liu, 1997). Parameter estimation in the post-migrated domain, usually referred to as migration velocity analysis (MVA), consists of two main steps: (1) prestack depth migration with a trial velocity model, and (2) parameter update designed to minimize the residual moveout of events in the image gathers after the next prestack depth migration is applied. These two steps are iterated until the events in the image gathers are sufficiently flat. Note that MVA is quite robust in the presence of random noise because migration improves the signal-to-noise ratio (Gardner et al., 1974; Liu, 1997).

The parameter-estimation methodology employed here is based on the results of Sarkar and Tsvankin (2003). Although depth imaging of P-wave data requires knowledge of the five parameters listed above (V_{P0}, k_z, k_x, ϵ, and δ) in each block, Sarkar and Tsvankin (2003) show that for models without significant dips above the target, the moveout of events in image gathers is governed by the following four parameter combinations:

1) The NMO velocity at a certain point on the surface of the factorized layer or block: $V_{\rm nmo} \equiv V_{P0}\sqrt{1+2\delta}$
2) The vertical velocity gradient k_z
3) The lateral velocity gradient combined with the parameter δ: $\hat{k}_x = k_x\sqrt{1+2\delta}$
4) The anellipticity parameter η

If prestack migration is performed with the correct values of $V_{\rm nmo}$, k_z, $\hat{k}_x$, and η, the image gathers for reflections from both horizontal and dipping interfaces are flat. As illustrated by Figure 1, this conclusion remains valid even for uncommonly strong anisotropy (ϵ and δ) and heterogeneity (k_x and k_z). To decouple the horizontal gradient k_x from the coefficient δ and determine the other anisotropic coefficient ϵ, the velocity V_{P0} has to be known at a certain point within the factorized block (Sarkar and Tsvankin, 2003).

After discussing the minimum information required to estimate the parameters of factorized VTI media, we introduce the MVA methodology that includes nonhyperbolic moveout analysis on image gathers. The accuracy of the algorithm and its robustness in the presence of random noise are assessed by synthetic tests for a single layer and a multilayered factorized VTI medium. We outline different ways to specify the vertical velocity V_{P0} and analyze the influence of errors in V_{P0} on the inverted values of the other parameters and on the quality of the migrated image.

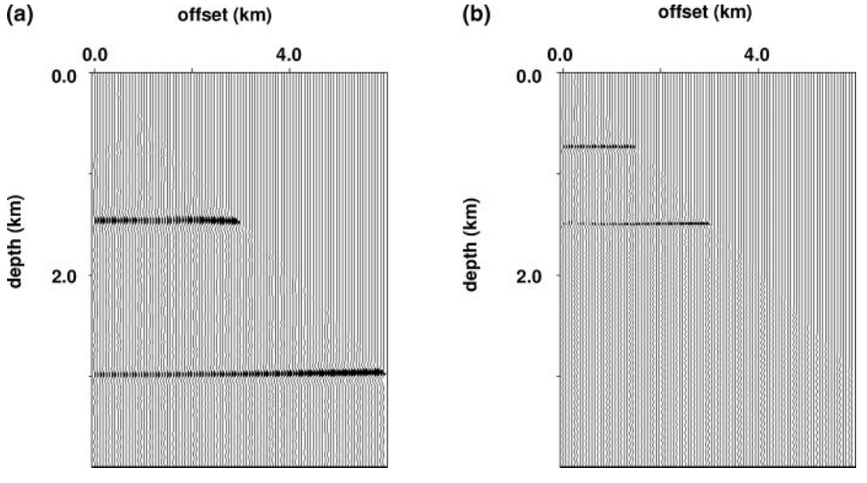

Figure 1. P-wave image gathers for two planar reflectors embedded in a factorized $v(x, z)$ VTI medium. The shallow reflector is dipping at 45°, the deep reflector is horizontal. The gathers are obtained after prestack migration for (a) the true model with the parameters $V_{P0,T} = 2000$ m/s, $k_{z,T} = 1.0\,{\rm s}^{-1}$, $k_{x,T} = 1.0\,{\rm s}^{-1}$, $\epsilon_T = 0.3$, and $\delta_T = 0.1$; (b) a model that has significantly distorted parameters $V_{P0,M} = 1000$ m/s, $k_{x,M} = 0.5\,{\rm s}^{-1}$, $\epsilon_M = 2.7$, and $\delta_M = 1.9$, but the correct $V_{\rm nmo}$, k_z, $\hat{k}_x$ and η. Uncommonly large values of ϵ_M, δ_M, and $k_{x,T}$ were chosen intentionally to show that the moveout in image gathers is controlled by $V_{\rm nmo}$, k_z, $\hat{k}_x$ and η for any strength of anisotropy and heterogeneity. Although both events on section (b) are flat, they are imaged at half the true depth because $V_{P0,M} = 0.5V_{P0,T}$.

PARAMETER ESTIMATION IN A FACTORIZED VTI LAYER

Here, we use the results of Sarkar and Tsvankin (2003) to evaluate the feasibility of estimating the parameters of a factorized VTI layer from P-wave reflection data. By replacing the actual factorized $v(x, z)$ model with narrow vertical strips of factorized $v(z)$ media, Sarkar and Tsvankin (2003) demonstrate that the moveout of a horizontal event in an image gather is governed by the effective values of the NMO velocity and the parameter η:

$$v^2_{\rm nmo}(x, t_0) = V^2(x)(1 + 2\delta)\frac{e^{k_z t_0} - 1}{k_z t_0}, \quad (1)$$

$$\hat{\eta}(x, t_0) = \frac{1}{8}\left[\frac{(1 + 8\eta)(e^{2k_z t_0} - 1)k_z t_0}{2(e^{k_z t_0} - 1)^2} + 1\right]; \quad (2)$$

$V(x) \equiv V_{P0} + k_x x$ is the vertical P-wave velocity at the surface, and $t_0 \equiv t_0(x, z)$ is the zero-offset time at location x from a horizontal reflector at depth z.

If long-offset data needed to constrain $\hat{\eta}$ (Grechka and Tsvankin, 1998) have been acquired, moveout analysis of a single event can yield estimates of both $v_{\rm nmo}(x, t_0)$ and $\hat{\eta}(x, t_0)$. Next, suppose that P-wave traveltimes from two horizontal reflectors sufficiently separated in depth are available. Then the ratio of the NMO velocities for these two events ($v_{\rm nmo,1}$ and $v_{\rm nmo,2}$) can be used to find [equation (1)]

$$\frac{v^2_{\rm nmo,1}(x, t_{0,1})}{v^2_{\rm nmo,2}(x, t_{0,2})} = \frac{t_{0,2}(e^{k_z t_{0,1}} - 1)}{t_{0,1}(e^{k_z t_{0,2}} - 1)}, \quad (3)$$

where $t_{0,1}$ and $t_{0,2}$ are the zero-offset times for the two events. According to equation (3), conventional hyperbolic moveout analysis of two horizontal events located in the same factorized block can provide an estimate of the vertical gradient k_z. Knowledge of k_z and the zero-offset time t_0 is sufficient for obtaining the anellipticity parameter η from equation (2) applied to one or both reflection events. The remaining two key quantities, $V_{\rm nmo} = V_{P0}\sqrt{1 + 2\delta}$ and $\hat{k}_x = k_x\sqrt{1 + 2\delta}$, can then be computed from equation (1), if the effective NMO velocities are determined at two or more locations x.

We conclude that the moveout of horizontal events at two different depths and two image locations may provide enough information to estimate the parameters $V_{\rm nmo}$, k_z, $\hat{k}_x$, and η. For the special case of a factorized $v(z)$ medium with a constant vertical gradient k_z, the moveout of two horizontal events at a single image location can be inverted for the parameters $V_{\rm nmo}$, k_z, and η.

As shown in Sarkar and Tsvankin (2003), reflection moveout of dipping events in factorized $v(x, z)$ VTI media is controlled by the same parameters ($V_{\rm nmo}$, k_z, $\hat{k}_x$, and η) as that of horizontal events. Most importantly, NMO velocity of events dipping at 25°–30° or more is highly sensitive to the parameter η (Alkhalifah and Tsvankin, 1995; Tsvankin, 2001), whereas the inversion of nonhyperbolic moveout from horizontal reflectors for η may suffer from instability (Grechka and Tsvankin, 1998). Therefore, the inclusion of dipping events in velocity analysis is helpful in obtaining accurate estimates of η; also, dip-dependent reflection moveout provides additional information about the parameters $V_{\rm nmo}$, k_z, and $\hat{k}_x$.

Still, even if both horizontal and dipping events are available, the parameters V_{P0}, k_x, ϵ, and δ remain generally unconstrained by P-wave reflection traveltimes. In particular, the vertical velocity V_{P0} is needed to define the depth scale of the VTI model in the migration of P-wave data. Hence, to build an anisotropic model for depth imaging, at least one medium parameter must be known a priori. Unless specified otherwise, the velocity V_{P0} in the synthetic data examples below is assumed known at some location on the surface of each factorized layer. Given this information about V_{P0}, velocity analysis of P-wave data can yield estimates of the parameters k_x, ϵ, and δ.

ALGORITHM FOR MIGRATION VELOCITY ANALYSIS

Inversion of seismic data is a nonlinear problem that can be solved through an iterative application of migration and velocity updating. Migration creates an image of the subsurface for trial values of the medium parameters, and then velocity analysis is used to update the model for the next run of the migration code. This iterative procedure, conventionally called MVA, is continued until a certain criterion (e.g., small residual moveout of events in image gathers) is satisfied.

Here, we apply anisotropic prestack depth migration [the migration algorithm is described in detail in Sarkar and Tsvankin (2003)] and tomographic velocity update to P-wave data acquired over the subsurface composed of factorized $v(x, z)$ VTI blocks. The iterations are stopped when the residual moveout for at least two reflectors in each factorized block is close to zero (i.e., the migrated depth for different offsets stays the same to within a specified fraction of the wavelength). The overall organization of our MVA algorithm is similar to that developed by Liu (1997) for isotropic media, but the VTI model is characterized, for P-waves, by two additional parameters: ϵ and δ.

The tomographic update of the medium parameters is based entirely on the residual moveout of events in image gathers. For horizontal reflectors embedded in a weakly anisotropic homogeneous VTI medium, the migrated depth z_M as a function of the half-offset h can be written as (Sarkar and Tsvankin, 2003):

$$z^2_M(h) \approx z^2_M(0) + h^2 V^2_{P0,M}\left(\frac{1}{V^2_{\rm nmo,T}} - \frac{1}{V^2_{\rm nmo,M}}\right) + \frac{2h^4}{h^2 + z^2_T}\left(\eta_M \frac{V^2_{\rm nmo,T}}{V^2_{\rm nmo,M}} - \eta_T \frac{V^2_{\rm nmo,M}}{V^2_{\rm nmo,T}}\right), \quad (4)$$

where the subscripts T and M denote the true and migration medium parameters, respectively, and z_T is the true zero-offset depth of the reflector. Equation (4) is nonhyperbolic and governed by two independent parameters: $V_{\rm nmo}$ and η. The NMO velocity $V_{\rm nmo}$ controls the hyperbolic (described by the h^2 term) part of the moveout curve and also contributes to the nonhyperbolic (h^4) term, while η influences nonhyperbolic moveout only. A similar closed-form expression is not available for dipping reflectors, but both the hyperbolic and nonhyperbolic portions of the residual moveout curve for dipping events depend on $V_{\rm nmo}$ and η (Sarkar and Tsvankin, 2003).

As discussed above, the residual moveout of P-waves in factorized $v(x, z)$ VTI media is a function of the parameters $V_{\rm nmo}$, k_z, $\hat{k}_x$, and η. Although it is difficult to express the migrated depth z_M in laterally heterogeneous media analytically in terms of these parameters, the residual moveout equation can be cast

in a form similar to that in equation (4):

$$z_M^2(h) \approx z_M^2(0) + Ah^2 + B\frac{h^4}{h^2 + z_M^2(0)}; \qquad (5)$$

A and B are dimensionless constants that describe the hyperbolic and nonhyperbolic portions of the moveout curve, respectively. Numerical tests (see below) confirm that the functional form in equation (5) with fitted coefficients A and B provides a good approximation for P-wave moveout in long-spread image gathers.

To apply equation (5) in velocity analysis, we first pick an approximate value of the zero-offset reflector depth $z_M(0)$ on the migrated stacked section. The parameters A and B are obtained by a 2D semblance scan on image gathers at each migrated zero-offset depth point. The best-fit combination of A and B that maximizes the semblance value is substituted into equation (5) to evaluate the residual moveout. It should be emphasized that the coefficients A and B in our algorithm are not directly inverted for the parameters $V_{\rm nmo}, k_z, \hat{k}_x$, and η. Rather, the only role of A and B is in providing an adequate functional approximation for $z_M(h)$.

After estimating the residual moveout in image gathers, we update the N-element parameter vector $\boldsymbol{\lambda}$ using the algorithm described in Appendix A. The update $\boldsymbol{\Delta\lambda}$ of the parameter vector is obtained by solving the system of linear equations,

$$\mathbf{A^T A \Delta\lambda} = \mathbf{A^T b}. \qquad (6)$$

$\mathbf{A}$ is a matrix with $M \times P$ rows (M is the number of offsets and P is the total number of image gathers used in the velocity analysis) and N columns that includes the derivatives of the migrated depth with respect to the medium parameters. The superscript T denotes the transpose, and $\mathbf{b}$ contains the migrated depths that define the residual moveout. The full definitions of the matrix $\mathbf{A}$ and vector $\mathbf{b}$ are given in Appendix A.

Each iteration of the MVA algorithm consists of the following four steps:

1) Prestack depth migration with a given estimate of the medium parameters
2) Picking along two reflectors in each VTI block to delineate the reflector shapes
3) Semblance scanning using equation (5) to estimate A and B for image points along each reflector
4) Application of equation (6) to update the medium parameters in such a way that the variance of the migrated depths as a function of offset is minimized (see Appendix A for more details about the minimization procedure)

Steps 1–4 are repeated until the magnitude of residual moveout of events in image gathers becomes sufficiently small.

EXAMPLE WITH A SINGLE FACTORIZED LAYER

First, we consider two irregular reflectors embedded in a factorized $v(x, z)$ VTI medium with $k_z > k_x > 0$ and a positive value of η typical for shale formations (Figure 2). For the first application of prestack depth migration, we choose a homogeneous, isotropic medium ($V_{P0} = 2600$ m/s, $k_z = k_x = \epsilon = \delta = 0$) as the initial velocity model. The migrated stacked image (Figure 3a) obtained using offsets extending to a maximum offset-to-depth ratio of two is clearly inferior to the true image in Figure 2. We start the velocity-updating process by manually picking along both imaged reflectors to outline their shapes. Then equation (5) is used to compute two-parameter semblance scans for each reflector and evaluate the residual moveout in the image gathers.

One such semblance scan computed for the shallow reflector at the midpoint 3.5 km is displayed in Figure 3b. The values of A and B that correspond to the maximum semblance coefficient in Figure 3b provide an accurate description of residual moveout at this location. Although a certain degree of tradeoff exists between A and B, any pair of values inside the innermost semblance contour gives almost the same variance of the migrated depths. Note that the interplay between A and B is similar to that between the NMO velocity and parameter η in the inversion of P-wave nonhyperbolic reflection moveout (Grechka and Tsvankin, 1998; Tsvankin, 2001).

For purposes of velocity analysis, we use the image gathers at 12 equally spaced surface locations between 3 km and 4.2 km. The maximum offset-to-depth ratio for the selected image gathers at the shallow reflector is close to two, which is marginally suitable for estimating the parameter η. Tighter constraints on η are provided by the NMO velocities of reflections from the dipping segments of the shallow reflector (the dips exceed 30° in the middle of the section).

After the residual moveout has been evaluated, we fix the vertical velocity $V_{P0}\,(x = 3000$ m, $z = 0) = 2600$ m/s at the correct value and update the parameters k_z, k_x, ϵ, and δ using equation (6). The stacked images after four (Figure 4a) and eight (Figure 4b) iterations illustrate the improvements in the focusing and positioning of both reflectors during the velocity update. The magnitude of the residual moveout for both reflectors decreases as the model parameters converge toward their actual values (Figure 5).

The inverted model parameters are close to the correct values: $k_z = 0.61 \pm 0.02$ s^{-1}, $k_x = 0.2 \pm 0.0$ s^{-1}, $\epsilon = 0.11 \pm 0.01$, and

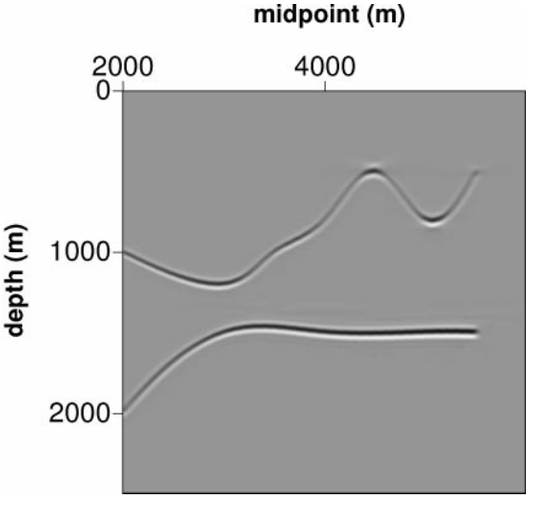

Figure 2. True image of two reflectors embedded in a factorized $v(x, z)$ VTI medium with the parameters $V_{P0}(x = 3$ km, $z = 0) = 2600$ m/s, $k_z = 0.6$ s^{-1}, $k_x = 0.2$ s^{-1}, $\epsilon = 0.1$, and $\delta = -0.1$. The corresponding effective parameters are $V_{\rm nmo}\,(x = 3$ km, $z = 0) = 2326$ m/s, $k_z = 0.6$ s^{-1}, $\hat{k}_x = 0.18$ s^{-1}, and $\eta = 0.25$. To obtain the stacked images shown in Figures 2, 3a, 4, 6, and 7b, we used a maximum offset of 2 km.

$\delta = -0.11 \pm 0.01$. The error bars were computed by assuming a standard deviation of ± 5 m in picking migrated depths on the selected image gathers and substituting this picking error into equation (6) to find the corresponding deviations of the model parameters near the actual solution.

Next, we apply the MVA method with an erroneous value of $V_{P0}\,(x = 3\text{ km}, z = 0) = 2000$ m/s, which is 23% smaller than the true vertical velocity (2600 m/s). The stacked images of both reflectors obtained after the velocity analysis (Figure 6a) are well focused, which indicates that the image gathers have been flattened. Indeed, although the estimated medium parameters listed in the caption of Figure 6 are distorted, the effective parameters responsible for the residual moveout are close to their actual values: $V_{\rm nmo}\,(x = 3\text{ km}, z = 0) = 2315$ m/s, $k_z = 0.58\text{ s}^{-1}$, $\hat{k}_x = 0.17\text{ s}^{-1}$, and $\eta = 0.25$.

This result corroborates the analysis of residual moveout in Sarkar and Tsvankin (2003) and confirms that our algorithm converges toward the correct parameters $V_{\rm nmo}$, k_z, $\hat{k}_x$, and η, even if the vertical velocity V_{P0} on the surface of the layer is poorly known. However, since V_{P0} assumed in the velocity analysis is too low, both reflectors in Figure 6a are imaged at depths that are about 23% smaller than the actual ones in Figure 6b. The depth distortion also leads to the rotation of the

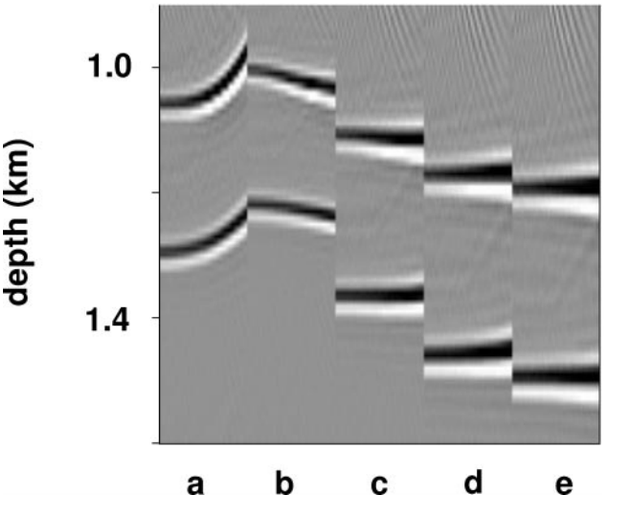

Figure 5. Residual moveout in image gathers for both reflectors in the model in Figure 2 at the surface location 3 km: (a) for the initial model; (b) after two, (c) four, (d) six, and (e) eight iterations. The velocity updating was stopped after eight iterations.

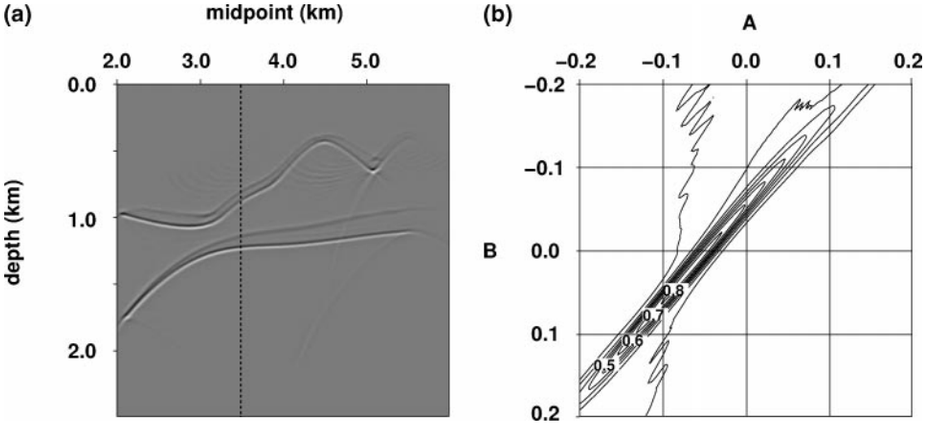

Figure 3. (a) Image of the model from Figure 2 obtained using a homogeneous isotropic velocity field with $V_{P0} = 2600$ m/s. (b) Semblance contour plot computed from equation (5) for the shallow reflector at the surface location 3.5 km [marked by the dashed vertical line in (a)].

Figure 4. Stacked image for the model in Figure 2 after (a) four iterations, and (b) eight iterations of prestack migration velocity analysis.

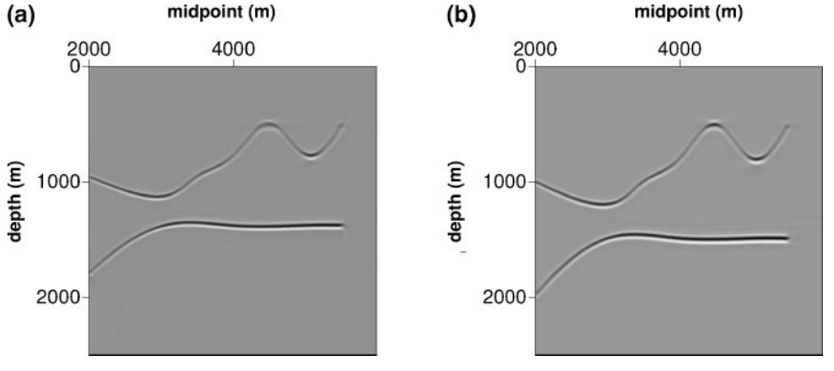

dipping segments of the reflecting interfaces, which is discussed in more detail below.

SENSITIVITY TO NOISE AND REFLECTOR SEPARATION

To evaluate the influence of noise on the estimation of the medium parameters and the quality of imaging, we added Gaussian noise to the data set from Figure 2. The signal-to-noise ratio, measured as the ratio of the peak amplitude of the signal to the root-mean-square (rms) amplitude of the background noise, is close to one, and the frequency bands of the noise and signal are identical (Figure 7a). The estimates of the medium parameters obtained after the migration velocity analysis with the correct value of V_{P0} at the surface location 3 km are quite accurate: $k_z = 0.52 \pm 0.07\ \mathrm{s}^{-1}$, $k_x = 0.2 \pm 0.01\ \mathrm{s}^{-1}$, $\epsilon = 0.13 \pm 0.03$, and $\delta = -0.07 \pm 0.03$. The error bars were computed in the same way as those for the noise-free synthetic example above (Figure 4), but the depth-picking error for all offsets and image locations was assumed to be 20 m instead of 5 m. Clearly, even the severe noise contamination did not cause measurable errors in the medium parameters or noticeable distortions in the stacked image (Figure 7b).

The robustness of the migration velocity analysis employed here in the presence of random noise is not surprising. One aiding factor is that the MVA operates on migrated data, which have a higher signal-to-noise ratio than the original records because of partial stacking applied to the data during the migration step. Also, the semblance (coherency) operator used to evaluate the residual moveout on image gathers helps to suppress remaining random noise in the migrated data.

Accurate estimation of the vertical gradient k_z, and then the NMO velocity at the surface of the factorized layer, requires a sufficiently large difference between the NMO velocities of the two events used in the velocity analysis [see equation (3)], which implies that the corresponding reflectors should be well separated in depth. Figure 8 illustrates the dependence of the error in the vertical gradient k_z on the distance d between the two reflectors embedded in a factorized $v(x, z)$ medium.

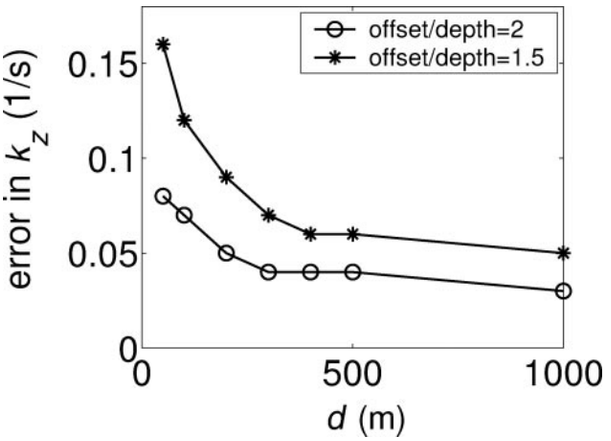

Figure 8. Influence of the vertical distance d between the two horizontal reflectors used in the velocity analysis on the absolute error in the vertical gradient k_z. The depth of the shallow reflector is 1 km; the maximum offset is 2 km for the upper curve and 1.5 km for the lower curve. The model parameters are $V_{P0}\,(x = 3\,\mathrm{km}, z = 0) = 2600$ m/s, $k_z = 0.6\ \mathrm{s}^{-1}$, $k_x = 0.2\ \mathrm{s}^{-1}$, $\epsilon = 0.2$, and $\delta = 0.1$. The vertical velocity at one location on the surface was held at the correct value.

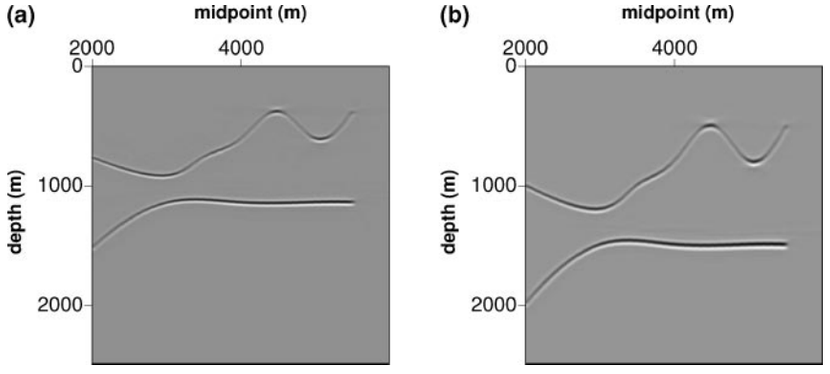

Figure 6. (a) Stacked image obtained after velocity analysis with the wrong value of the vertical velocity $V_{P0}\,(x = 3$ km, $z = 0) = 2000$ m/s. The estimated medium parameters are $k_z = 0.58\ \mathrm{s}^{-1}$, $k_x = 0.15\ \mathrm{s}^{-1}$, $\epsilon = 0.51$, $\delta = 0.17$. (b) Stacked image for the correct medium parameters (Figure 2). Since V_{P0} in (a) is smaller than the true value, both reflectors are shifted up with respect to their correct positions in (b).

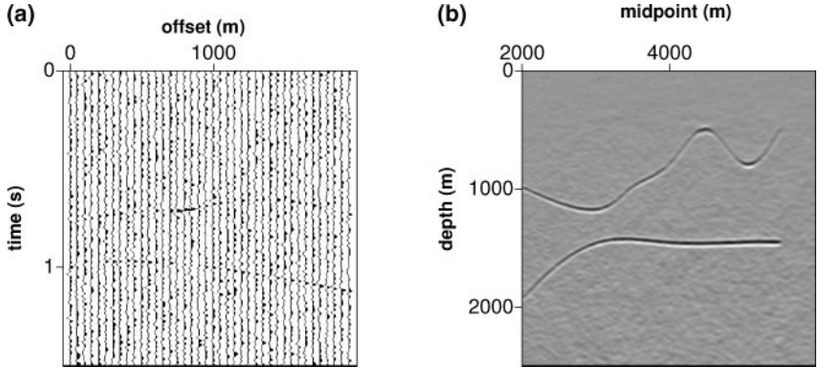

Figure 7. Influence of noise on the velocity analysis and migration: (a) a shot gather from the data set in Figure 2 after the addition of Gaussian noise (the signal-to-noise ratio is one), (b) the image obtained for the noisy data set.

The depth of the shallow reflector is fixed at 1000 m, while the depth of the second reflector ranges from 1050 to 2000 m. The velocity analysis operated with the residual moveout on 12 image gathers (with 20 offsets each) whose horizontal coordinates span a distance of 1200 m. The error in k_z was computed from equation (6) assuming that the error in picking the migrated depths is ± 5 m.

After an initial decrease with the distance d, the error in k_z becomes almost constant as d approaches 500 m. For a maximum offset-to-depth ratio (at the shallow reflector) of two, the error curves flatten out for $d \approx 250$ m, which is equal to one-fifth of the depth of the bottom reflector. If the maximum offset-to-depth ratio is 1.5, the curve flattens out for a larger depth $d \approx 350$ m (approximately one-quarter of the depth of the bottom reflector). Since the parameters ϵ and δ are computed using the estimated value of k_z, the errors in ϵ and δ have a similar dependence on d. Note that the minimum suitable vertical distance d found here is close to the minimum layer thickness conventionally assumed in interval velocity estimation based on the Dix equation.

The errors in all parameters reduce with increasing number of offsets in the image gathers, which can influence the sensitivity estimates. Although the results of the error analysis also vary with the anisotropic coefficients ϵ and δ and the velocity gradients, this dependence is not significant if the velocity update is performed with reasonable constraints on the model parameters.

TEST FOR A MULTILAYERED MODEL

Next, we apply the algorithm to the three-layer model shown in Figure 9. Each layer contains two reflecting interfaces, as requried in our method, with every second reflector serving as the boundary between layers. The first and third layers are vertically heterogeneous $[v(z)]$ and isotropic, while the second layer is a factorized, laterally heterogeneous $[v(x, z)]$ medium. All interfaces are quasi-horizontal, with the largest dips (at the flanks of the syncline) of 10° or less. The model is designed to represent a typical depositional environment in the Gulf of Mexico, where anisotropic shale layers (the middle layer in Figure 9) are often embedded between isotropic sands.

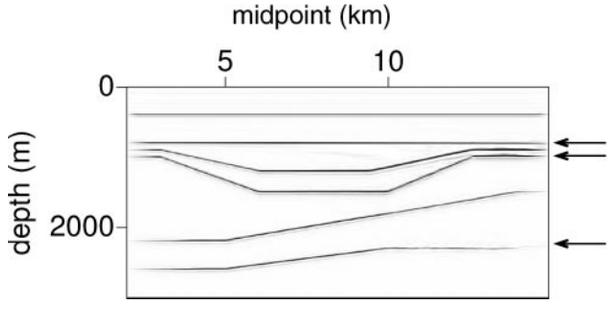

Figure 9. True image of a three-layer factorized medium. Every second reflector (indicated here with arrows) represents the bottom of a layer. The parameters of the first subsurface layer are $V_{P0}\,(x = 4000$ m, $z = 0) = 1500$ m/s, $k_z = 1.0\,\mathrm{s}^{-1}$, and $k_x = \epsilon = \delta = 0$; for the second layer, $V_{P0}\,(x = 4000$ m, $z = 800$ m$) = 2300$ m/s, $k_z = 0.6$ s^{-1}, $k_x = 0.1$ s^{-1}, $\epsilon = 0.1$, and $\delta = -0.1$; for the third layer, $V_{P0}(x = 4000$ m, $z = 1162$ m$) = 2718$ m/s, $k_z = 0.3$ s^{-1}, and $k_x = \epsilon = \delta = 0$. To obtain the stacked images shown in Figures 9, 11, 13, and 17, we used a maximum offset of 4 km.

For the velocity analysis we use image gathers located along the left flank of the syncline with the midpoints ranging from 4400 m to 5600 m; the maximum offset-to-depth ratio for the image gathers is close to two. The medium parameters are estimated in the layer-stripping mode starting at the surface. For the first (top) layer, the vertical velocity is assumed to be known at a single surface location [$V_{P0}\,(x = 4000$ m, $z = 0$ m $= 1500$ m/s], which is sufficient for obtaining accurate values of k_z, k_x, ϵ, and δ (Figure 10).

To estimate the medium parameters in the second and third layers, we need to fix the vertical velocity at a certain spatial location in each layer. Three different scenarios for choosing V_{P0} in the second and third layers are examined below.

V_{P0} at the top of each layer is known

Suppose a vertical borehole was drilled at the surface location 4000 m, and the vertical velocity at the top of the second and third layers was measured from sonic logs or check shots. Prestack depth migration with the estimated parameters of the first layer yields the depth of the top of the second layer at the surface location 4000 m. Using the correct value of the vertical velocity at this point $V_{P0}\,(x = 4000$ m, $z = 800$ m$) = 2300$ m/s, we carry out the parameter estimation for the second layer, and then repeat the same procedure for the third layer with the velocity $V_{P0}\,(x = 4000$ m, $z = 1162$ m$) = 2718$ m/s.

The velocity analysis results in highly accurate estimates of all four parameters (k_z, k_x, ϵ, and δ) in the second and third layers. The shapes and depths of the reflectors imaged for the reconstructed velocity model (Figure 11) are practically

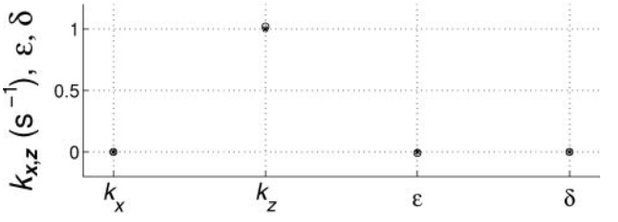

Figure 10. Estimated ($\circ$) and true ($\star$) parameters of the first layer obtained using the correct $V_{P0}\,(x = 4000$ m, $z = 0) = 1500$ m/s at the surface.

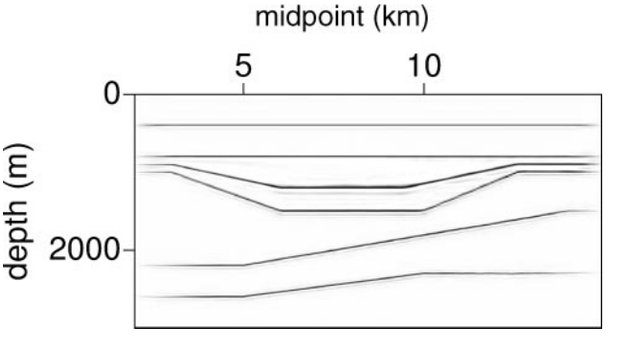

Figure 11. Stacked image for the model from Figure 9 obtained after prestack depth migration with estimated medium parameters. The vertical velocity V_{P0} at the top of each layer was known.

indistinguishable from those on the true section (Figure 9). This test confirms that migration velocity analysis in layered factorized $v(x, z)$ VTI media can be used to invert for the the velocity gradients k_z and k_x and the anisotropic coefficients ϵ and δ if the vertical velocity is known at a single point in each layer.

V_{P0} in the second layer is incorrect

Now suppose that the vertical velocity V_{P0} ($x = 4000$ m, $z = 800$ m) used for the top of the second layer has error (2600 m/s instead of 2300 m/s). Although this error in V_{P0} causes distortions in the inverted values of the other parameters (Figure 12), the effective quantities V_{nmo} ($x = 4000$ m, $z = 800$ m) $= 2080$ m/s, $k_z = 0.56$ s^{-1}, $\hat{k}_x = 0.09$ s^{-1}, and $\eta = 0.23$ do not significantly differ from the true values, which corroborates our results for a single layer (Figure 6). Since the assumed value of V_{P0} ($x = 4000$ m, $z = 800$ m) is higher than the correct velocity, the second layer is stretched in depth by about 13%, and the bottom of the syncline is imaged at a depth that is 80 m too large (Figure 13). This depth stretch in the second layer also causes a tilt of the syncline's flanks whose dips in Figure 13 exceed the true values.

To continue the velocity analysis, we use the correct vertical velocity at the imaged top of the third layer. Despite the depth shift of the third layer, the algorithm yields accurate values of all four interval parameters (Figure 14). Because of the depth and dip distortions in the second layer, the two bottom reflectors are imaged at somewhat greater depths and are slightly deformed (Figure 13). In particular, on the left side of the section the fifth and sixth reflectors are no longer horizontal; they have acquired mild dips to conform to the stretched synclinal structure above. It should be mentioned that if the error in the vertical velocity in the second layer becomes large, the distortions in the reflector shapes may be so significant that errors in the parameters of the third layer will no longer be negligible.

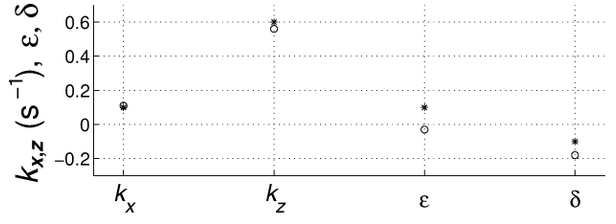

Figure 12. Estimated (○) and true (⋆) parameters of the second layer obtained with an inaccurate value of the vertical velocity at the top of that layer [V_{P0} ($x = 4000$ m, $z = 800$ m) $= 2600$ m/s].

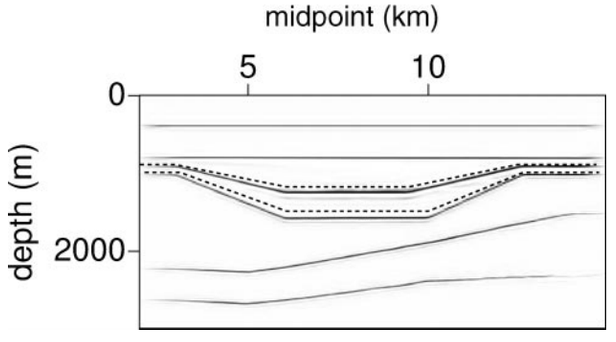

Figure 13. Stacked image obtained after prestack depth migration using the estimated parameters from Figures 10, 12, and 14. The vertical velocity V_{P0} at the top of the second layer was inaccurate. The dashed lines mark the true reflector positions in the second layer.

V_{P0} is continuous across the interfaces

If no borehole information is available, one assumption that might be made is that the velocity V_{P0} is a continuous function of depth at a certain horizontal coordinate. To identify this point of continuity at the boundary between the first and second layers, we examine the moveout along the third and fourth reflectors (only for offsets smaller than 1000 m) after migration with an isotropic homogeneous velocity field in the second layer. The migration velocity was chosen to be equal to the true velocity at the bottom of the first layer (i.e., at the second reflector). To select the point of continuity, we pick the midpoint closest to the image gathers on the third and fourth reflectors that have the smallest residual moveout. This criterion yielded $x = 3900$ m, which is sufficiently close to the true point of continuity for the second reflector ($x = 4000$ m). Using the estimated vertical velocity at $x = 3900$ m [V_{P0} ($x = 3900$ m, $z = 800$ m) $= 2316$ m/s], we determine the parameters of the second layer with sufficient accuracy (Figure 15).

Next, applying the criterion of minimum residual moveout, we find the point of continuity between the second and third layers ($x = 5937$ m, $z = 1483$ m). Although the estimated continuity point is shifted by 1000 m from its true location, the results of the velocity analysis for the third layer (Figure 16) are quite satisfactory, and the imaged reflectors are well focused and properly positioned (Figure 17).

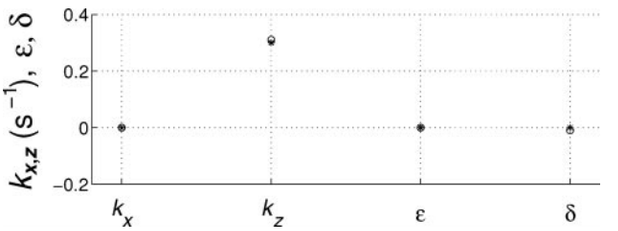

Figure 14. Estimated (○) and the true (⋆) parameters of the third layer obtained with an inaccurate value of the vertical velocity at the top of the second layer [V_{P0} ($x = 4000$ m, $z = 800$ m) $= 2600$ m/s]. The vertical velocity at the top of the third layer was correct [V_{P0} ($x = 4000$ m, $z = 1208$ m) $= 2732$ m/s].

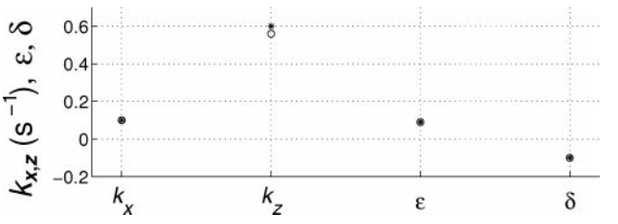

Figure 15. Estimated (○) and true (⋆) parameters of the second layer obtained assuming that V_{P0} is continuous between the first and second layers at the point ($x = 3900$ m, $z = 1208$ m).

In the absence of borehole data, the assumption of continuous vertical velocity provides a practical way to build an anisotropic heterogeneous model for prestack migration. Depending on the complexity of the model and the value of δ, however, the point of continuity may be estimated with a substantial lateral shift or may not exist at all. Still, our tests show that for models without steep dips or strong heterogeneity, an error in identifying the point of continuity does not distort the effective parameters $V_{\rm nmo}, k_z, \hat{k}_x$, and η. Therefore, the migrated section would still be well focused, although the imaged reflectors would be subject to a depth stretch.

DISCUSSION AND CONCLUSIONS

Approximating heterogeneous VTI models by factorized blocks or layers with linear velocity variation provides a convenient way to reconstruct anisotropic velocity fields for P-wave prestack depth imaging. The MVA algorithm introduced here estimates the anisotropic parameters and velocity gradients in each block by minimizing the residual moveout of P-wave reflections in image gathers.

For both horizontal and dipping events, the residual moveout is governed by four effective parameters: the NMO velocity $V_{\rm nmo}$ at the surface of the factorized block, the vertical velocity gradient k_z, the quantity $\hat{k}_x = k_x\sqrt{1+2\delta}$ that contains the lateral velocity gradient k_x and Thomsen's parameter δ, and the anellipticity parameter η. Application of our MVA method confirms the conclusion of Sarkar and Tsvankin (2003) that stable recovery of the parameters $V_{\rm nmo}$, k_z, $\hat{k}_x$, and η requires reflection moveout from at least two interfaces within each block sufficiently separated in depth. Numerical tests indicate that the vertical distance between the two reflectors should exceed one-quarter of the depth of the bottom reflector. Another condition, essential for the stable estimation of the parameter η, is either the presence of dipping interfaces (dips should exceed 25°) or acquisition of long-spread data from subhorizontal reflectors providing maximum offset-to-depth ratios of at least two.

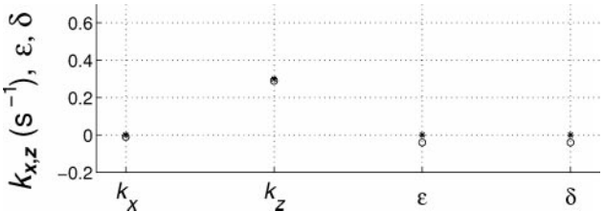

Figure 16. Estimated (○) and true (⋆) parameters of the third layer obtained assuming that V_{P0} is continuous between the first and second layers at the point ($x = 3900$ m, $z = 1208$ m), and between the second and third layers at the point ($x = 5937$ m, $z = 1483$ m).

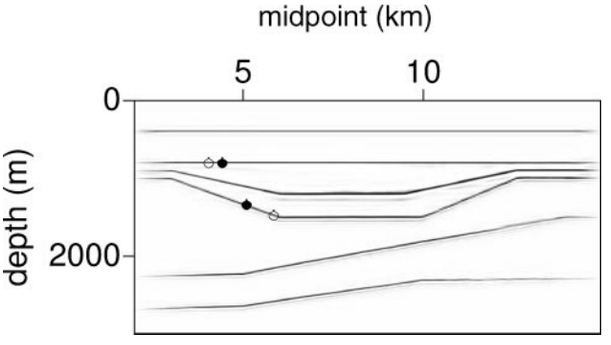

Figure 17. Stacked image obtained after prestack depth migration using the estimated parameters from Figures 10, 15, and 16. The vertical velocity was assumed to be continuous at the points marked by (○); the true points of continuity are marked by (●).

For such long-offset data, the residual moveout was described by a nonhyperbolic function that depends on two independent moveout parameters. Although these parameters are not directly used in the velocity analysis, their best-fit values found from semblance search give an accurate approximation for the residual moveout. The MVA is implemented in an iterative fashion, with the residual moveout minimized at each iteration step by solving a system of linear equations for the parameter updates. Since the parameter estimation is performed in the post-migrated domain, the algorithm is robust in the presence of random noise and does not lose accuracy for models with significant lateral heterogeneity and dipping structures.

The main problem in the application of P-wave velocity analysis for VTI media is that the vertical velocity V_{P0} (needed to build velocity models for depth migration) is generally unconstrained by P-wave reflection moveout (Alkhalifah and Tsvankin, 1995; Tsvankin, 2001; Grechka et al., 2002). Also, the lateral gradient k_x is always coupled to the anisotropy coefficient δ through the parameter $\hat{k}_x = k_x\sqrt{1+2\delta}$. A priori knowledge of V_{P0} at any single point in the factorized block, however, is sufficient for estimating the true lateral gradient k_x and, therefore, reconstructing the spatially varying vertical-velocity field, as well as the Thomsen anisotropic parameters ϵ and δ.

The vertical velocity sometimes can be estimated from borehole data using either check shots or sonic logs. Alternatively, as demonstrated by a synthetic example, a suitable model for depth imaging (in particular, for migration codes that require a smooth velocity field) can be constructed by assuming that V_{P0} is continuous across layer boundaries. With increasing level of structural complexity, however, the migration result becomes more sensitive to the lateral location of the assumed continuity point, and the adopted continuous velocity field may cause errors in the final image.

For relatively simple models with subhorizontal interfaces, an erroneous value of V_{P0} causes only a depth stretch that can vary from one layer to another. In the presence of dipping structures, errors in the vertical velocity also either increase (if V_{P0} is too high) or reduce (if V_{P0} is too low) the imaged dips. Such a depth stretch for dipping interfaces in the overburden can distort the shape of the underlying reflectors, even if the parameters immediately above these reflectors are estimated correctly. Still, the examples given above show that the moveout of events in image gathers is not influenced by an incorrect choice of V_{P0}, and the migrated image remains well focused (but possibly distorted) as long as the algorithm yields accurate values of $V_{\rm nmo}$, k_z, $\hat{k}_x$, and η.

This conclusion, however, breaks down if the section above the target contains interfaces with substantial dip or curvature. Then P-wave reflection moveout and, therefore, residual moveout on image gathers become dependent on V_{P0}, ϵ, and δ separately (Le Stunff et al., 2001; Grechka et al., 2002). As the dip of the intermediate interfaces increases, moveout on image gathers becomes more sensitive to errors in V_{P0}, ϵ, and

δ, although it does not necessarily mean that these parameters can be resolved from P-wave data alone (Grechka et al., 2002). For models of this type, the layer-stripping approach adopted in our MVA algorithm is not optimal because the Thomsen parameters of a given layer in some cases may be better constrained using reflection data from deeper interfaces (Le Stunff et al., 2001).

Application of the MVA method introduced here to field data will be discussed in a sequel paper.

ACKNOWLEDGMENTS

We are grateful to members of the A(nisotropy)-Team of the Center for Wave Phenomena (CWP), Colorado School of Mines, for helpful discussions and to Ken Larner for his careful review of the manuscript and useful suggestions. The reviews by the editors and referees of *Geophysics* helped to improve the paper. The support for this work was provided by the Consortium Project on Seismic Inverse Methods for Complex Structures at CWP and by the Chemical Sciences, Geosciences and Biosciences Division, Office of Basic Energy Sciences, U.S. Department of Energy.

APPENDIX A

ALGORITHM FOR VELOCITY UPDATE

Following the approach suggested by Liu (1997), we design the velocity-updating algorithm to minimize the variance in the migrated depths of events in image gathers. To simplify a generally nonlinear inverse (minimization) problem, we perform the velocity analysis iteratively, with a set of linear equations being solved at each iteration. Below we discuss the velocity update performed at a single (ℓth) step of the iterative process.

Suppose that prestack migration after the $(\ell-1)$th iteration of the velocity analysis resulted in the migrated depths $z_0(x_j, h_k)$ (x_j is the midpoint of the jth image gather, and h_k is the half-offset). Then, the migrated depths $z(x_j, h_k)$ after the ℓth iteration can be represented as a linear perturbation of $z_0(x_j, h_k)$:

$$z(x_j, h_k) = z_0(x_j, h_k) + \Sigma_{i=1}^{N} \frac{\partial z_0(x_j, h_k)}{\partial \lambda_i} \Delta\lambda_i, \quad \text{(A-1)}$$

where $\partial z_0(x_j, h_k)/\partial\lambda_i$ are the derivatives of the migrated depths with respect to the medium parameters λ_i ($i = 1, 2, 3, \ldots N$), and $\Delta\lambda_i = \lambda_i' - \lambda_i$ are the desired parameter updates. The goal of the updating procedure is to estimate $\Delta\lambda_i$ and, therefore, find the parameters λ_i' to be used for the migration after the ℓth iteration.

The variance V of the migrated depths for a single reflection event at all offsets and image gathers is

$$V = \Sigma_{j=1}^{P} \Sigma_{k=1}^{M} [z(x_j, h_k) - \hat{z}(x_j)]^2, \quad \text{(A-2)}$$

where $\hat{z}(x_j) = (1/M)\Sigma_{k=1}^{M} z(x_j, h_k)$ is the average migrated depth of the event at midpoint x_j, P is the number of image gathers used in the velocity update, and M is the number of offsets in each image gather. The minimization at each iteration step is accomplished by searching for the parameter updates that satisfy the condition $\partial V/\partial(\Delta\lambda_r) = 0$ $(r = 1, 2, 3, \ldots N)$. Subsituting equation (A-1) in equation (A-2), differentiating the variance with respect to the parameter updates, and setting $\partial V/\partial(\Delta\lambda_r) = 0$ yields

$$-\Sigma_{j=1}^{P}\Sigma_{k=1}^{M}\Sigma_{i=1}^{N}(g_{jk,i} - \hat{g}_{j,i})(g_{jk,r} - \hat{g}_{j,r})\Delta\lambda_i = \Sigma_{j=1}^{P}\Sigma_{k=1}^{M}[z_0(x_j, h_k) - \hat{z}_0(x_j)](g_{jk,r} - \hat{g}_{j,r}), \quad \text{(A-3)}$$

where $g_{jk,r} \equiv \partial z_0(x_j, h_k)/\partial\lambda_r$, $g_{jk,i} \equiv \partial z_0(x_j, h_k)/\partial\lambda_i$, and $\hat{g}_{j,i} \equiv (1/M)\Sigma_{k=1}^{M} g_{jk,i}$; all derivatives are evaluated for the medium parameters λ_i.

Equation (A-3) can be rewritten in matrix form as

$$\mathbf{A^T A \Delta\lambda} = \mathbf{A^T b}, \quad \text{(A-4)}$$

where $\mathbf{A}$ is a matrix with $M \times P$ rows and N columns whose elements are $g_{jk,r} - \hat{g}_{j,r}$, and $\mathbf{b}$ is a vector with $M \times P$ elements defined as $z_0(x_j, h_k) - \hat{z}_0(x_j)$. $\mathbf{A^T A}$ is a square $N \times N$ matrix, and the vector $\mathbf{A^T b}$ has N elements, so the problem has been reduced to a system of N linear equations with N unknowns $\mathbf{\Delta\lambda}$. We solve the system (A-4) using a linear conjugate gradient scheme to obtain $\mathbf{\Delta\lambda}$ and the updated parameters $\mathbf{\lambda' = \Delta\lambda + \lambda}$.

The derivatives of the depths $z(x_j, h_k)$ with respect to the medium parameters λ_i (and, therefore, the matrix $\mathbf{A}$) can be determined from the imaging equations (e.g., Liu, 1997; Sarkar and Tsvankin, 2003):

$$\tau_s(y, h, x, z, \boldsymbol{\lambda}) + \tau_r(y, h, x, z, \boldsymbol{\lambda}) = t(y, h), \quad \text{(A-5)}$$

$$\frac{\partial \tau_s(y, h, x, z, \boldsymbol{\lambda})}{\partial y} + \frac{\partial \tau_r(y, h, x, z, \boldsymbol{\lambda})}{\partial y} = \frac{\partial t(y, h)}{\partial y}. \quad \text{(A-6)}$$

Here y is the common-midpoint location at the surface, h is the half-offset, τ_s is the traveltime from the source location x_s ($x_s = y + h$) to the diffractor location (x, z) that was obtained after prestack depth migration with the medium parameters λ_i, τ_r is the traveltime from the receiver location x_r ($x_r = y - h$) to the point (x, z), and $t(y, h)$ is the observed reflection traveltime. Note that y, x, and z depend on the medium parameters λ_i, while h is an independent variable. Because x is fixed at the surface location where a particular image gather is analyzed, the derivative of x with respect to λ_i is set to zero.

Differentiating equation (A-5) with respect to λ_i gives

$$\left[\frac{\partial \tau_s}{\partial y} + \frac{\partial \tau_r}{\partial y}\right]\frac{dy}{d\lambda_i} + \left[\frac{\partial \tau_s}{\partial z} + \frac{\partial \tau_r}{\partial z}\right]\frac{dz}{d\lambda_i} + \left[\frac{\partial \tau_s}{\partial \lambda_i} + \frac{\partial \tau_r}{\partial \lambda_i}\right] = \frac{\partial t}{\partial y}\frac{dy}{d\lambda_i}. \quad \text{(A-7)}$$

Taking equation (A-6) into account simplifies equation (A-7) to

$$\left[\frac{\partial \tau_s}{\partial z} + \frac{\partial \tau_r}{\partial z}\right]\frac{dz}{d\lambda_i} = -\frac{\partial \tau_s}{\partial \lambda_i} - \frac{\partial \tau_r}{\partial \lambda_i}, \quad \text{(A-8)}$$

or

$$\frac{dz}{d\lambda_i} = -\left[\frac{\partial \tau_s}{\partial \lambda_i} + \frac{\partial \tau_r}{\partial \lambda_i}\right]\frac{1}{q_s + q_r}, \quad \text{(A-9)}$$

where $q_s = \partial\tau_s/\partial z$ and $q_r = \partial\tau_r/\partial z$ are the vertical slownesses evaluated at the diffractor for the specular rays connecting the diffractor with the source and the receiver, respectively.

To find the derivatives $dz/d\lambda_i$, we perform ray tracing using the prestack-migrated image after the $(\ell-1)$th iteration. First, the dip of the reflector needed to define the specular reflected

rays is estimated by manual picking on the image. Then, for a given diffraction point on the reflector and a fixed source-receiver offset, the specular ray is traced through two models, one of which is defined by the parameters λ_i and the other by parameters slightly deviating from λ_i (i.e., λ_i are slightly perturbed). The corresponding perturbation of the traveltime between the source and the diffractor is divided by the perturbation in λ_i to obtain $\partial\tau_s/\partial\lambda_i$, while the same quantity for the traveltime leg between the diffractor and the receiver gives $\partial\tau_r/\partial\lambda_i$. The slownesses q_r and q_s at the diffraction point are part of the output of the ray-tracing algorithm (Červený, 1972).

REFERENCES

Alkhalifah, T., 1997, Seismic data processing in vertically inhomogeneous TI media: Geophysics, **62**, 662–675.

Alkhalifah, T., Fomel, S., and Biondi, B., 2001, The space-time domain: Theory and modelling for anisotropic media: Geophysical Journal International, **144**, 105–113.

Alkhalifah, T., and Tsvankin, I., 1995, Velocity analysis for transversely isotropic media: Geophysics, **60**,1550–1566.

Červený, V., 1972, Seismic rays and ray intensities in inhomogeneous anisotropic media: Geophysical Journal of the Royal Astronomical Society, **29**, 1–13.

Gardner, G. H. F., French, W. S., and Matzuk, T., 1974, Elements of migration and velocity analysis: Geophysics, **39**, 811–825.

Grechka, V., and Tsvankin, I., 1998, Feasibility of nonhyperbolic moveout inversion in transversely isotropic media: Geophysics, **63**, 957–969.

——— 1999, 3-D moveout inversion in azimuthally anisotropic media with lateral velocity variation: Theory and a case study: Geophysics, **64**, 1202–1218.

Grechka, V., Pech, A., and Tsvankin, I., 2002, P-wave stacking-velocity tomography for VTI media: Geophysical Prospecting, **50**, 151–168.

Han, B., Galikeev, T., Grechka, V., Le Rousseau, J., and Tsvankin, I., 2000, A synthetic example of anisotropic P-wave processing for a model from the Gulf of Mexico, *in* Ikelle, L., and Gangi, A., eds., Anisotropy 2000: Fractures, converted waves and case studies: Proceedings of the Ninth International Workshop on Seismic Anisotropy (9IWSA): SEG.

Liu, Z., 1997, An analytical approach to migration velocity analysis: Geophysics, **62**, 1238–1249.

Le Stunff, Y., and Jeannot, J. P., 1998, Pre-stack anisotropic depth imaging: 60th Conference, European Association of Geoscientists and Engineers, Extended Abstracts.

Le Stunff, Y., Grechka, V., and Tsvankin, I., 2001, Depth-domain velocity analysis in VTI media using surface P-wave data: Is it feasible?: Geophysics, **66**, 897–903.

Sarkar, D., and Tsvankin, I., 2003, Analysis of image gathers in factorized VTI media: Geophysics, **68**, 2016–2025.

Stork, C., 1992, Reflection tomography in the post migrated domain: Geophysics, **57**, 680–692.

Thomsen, L., 1986, Weak elastic anisotropy: Geophysics, **51**, 1954–1966.

Tsvankin, I., 2001, Seismic signatures and analysis of reflection data in anisotropic media: Elsevier Science Publishing Company, Inc.